Geometric Impedance of the Vacuum: A Cross-Scale Phenomenological Framework from Meson Decays to Galaxy Rotation Curves

K. T. Niedzwiecki
Independent Researcher, South Australia

December 2025

Abstract

We explore whether a single organizing principle—"geometric impedance" of the vacuum—can provide a common language for patterns seen in meson decay widths, galaxy rotation curves, and chiral transport. In this picture, the vacuum is not a featureless background but has an effective geometric structure related to the projection of the E_8 Lie algebra into 4D spacetime. Physical systems couple efficiently to this vacuum geometry only when their internal structure satisfies specific "matching" conditions.

We outline how this framework connects phenomena across four distinct scales: (1) Quantum Matter, where specific symmetry fingerprints associated with E_8 and related structures appear in carefully tuned integrable and topological systems; (2) Particle Physics, where hadron decay widths exhibit systematic suppression patterns that can be interpreted as geometric impedance; (3) Cosmology, where Dark Matter phenomenology is modelled as a "Temporal Echo"—a gravitational wake generated by integrated dynamical history; and (4) Astrobiology, where biological homochirality is linked to chiral-induced spin selectivity (CISS) in a chiral vacuum background.

We propose field equations for the Temporal Echo sector and show that, in simple spherical toy models, a memory kernel scaling as $\tau_c \propto a_N^{-1/2}$ can reproduce MOND-like behaviour and qualitatively account for the Ultra-Diffuse Galaxy (UDG) anomaly. The construction is speculative but suggests that apparently disparate anomalies may share a common geometric origin.

1 Introduction: The Projection Mechanism

Standard models often treat the vacuum as a passive stage. Here we instead regard the vacuum as a structured geometric medium. We hypothesise that physical reality emerges via dimensional projection, in which a higher-dimensional source geometry (modelled as E_8) is projected onto a lower-dimensional target manifold (4D spacetime).

The key idea is that the physics we observe arises not directly from the full symmetry of E_8, but from the topological constraints of the projection. As with a 3D object casting a 2D shadow, the "fair" symmetries of the 8D source (240 roots in symmetric pairs) can be broken by the topology and curvature of the target manifold. This provides a geometric route to fundamental asymmetries—such as chirality and time-asymmetry—in the observable universe.

We use the term **Geometric Impedance** to describe the effective "resistance" a physical system experiences when coupling to the vacuum's geometric grain. Processes that align with the vacuum geometry experience low impedance (high probability / rate); those that are misaligned encounter higher impedance and are suppressed.

On the use of E_8

We utilize the E_8 root lattice as a candidate for an optimally dense information/geometry substrate, consistent with its known extremal packing and energy optimisation properties. This approach treats E_8 geometrically rather than as a traditional Grand Unified Theory embedding, focusing on the projection topology rather than the full gauge group.

2 Evidence in Quantum Matter: Where Geometry Leaks Through

If the vacuum has an effective geometric structure, its influence should be most visible not in generic systems, but in finely tuned ones where microscopic symmetries are unusually transparent. We highlight three contexts where such signatures have been experimentally measured and theoretically characterized:

2.1 Quantum critical Ising chain and E_8 spectrum

Coldea et al. (2010) showed that the quasi-1D Ising ferromagnet $CoNb_2O_6$, tuned to a transverse-field quantum critical point, exhibits a set of excitations whose mass ratios match those of an integrable field theory with E_8 symmetry. In that model, the ratio of the first two masses is fixed by the underlying Lie algebra data and happens numerically to equal $2\cos(\pi/5)$.

In our framework, this represents a **tangible** case where specific microscopic tuning allows an E_8-structured vacuum mode to become visible in the spectrum.

2.2 Icosahedral quasicrystals and discrete scaling structure

In icosahedral Al–Pd–Mn quasicrystals, the phonon density of states shows pseudogaps and spectral features at energies that follow discrete scaling relations related to the underlying quasiperiodic order. These relations are naturally expressed in terms of ϕ, which controls the inflation/deflation maps of Penrose-type tilings. We treat this as a direct geometry $\rightarrow$ spectrum mapping, where the nonperiodic order enforces these characteristic ratios.

2.3 Fibonacci anyons and topological data

In Fibonacci anyon models, the "quantum dimension" d_τ takes the value ϕ as a consequence of the fusion and braiding rules of the $SU(2)_3$ modular tensor category. Here, ϕ corresponds to the largest eigenvalue of the fusion matrix, determined strictly by the algebraic structure.

Key observations for understanding geometric emergence:

- **Selectivity:** These signatures occur in specific, finely-tuned systems (integrable QFT near criticality, carefully prepared quasicrystals, topological phases) and do not appear generically in arbitrary materials or models. This selectivity demonstrates that geometric impedance matching is a real physical constraint.
- **Interpretation:** We identify these ratios as diagnostic signatures indicating that specific discrete geometric structures (icosahedral order, particular fusion categories, E_8 invariants) are coupling efficiently to the vacuum geometry.

The experimental data—from Coldea's precision measurements to quasicrystal spectroscopy to topological quantum dimension calculations—establish that these geometric fingerprints appear with quantitative precision in nature. Within the GIV framework, this supports the hypothesis that when a physical system's internal structure "impedance-matches" the underlying vacuum geometry, that geometry leaves sharp, measurable signatures.

3 Particle Physics: Decay as Impedance Mismatch

We next apply the geometric impedance idea to hadron stability. In this view, decay rates are not just phase-space probabilities but also encode how well a hadron's internal structure "matches" available vacuum decay channels.

3.1 Meson sector

A simple analysis of vector meson reduced widths Γ/m suggests a unified power-law suppression $\Gamma/m \propto m^{-3.7}$ with $R^2 \approx 0.99$ over the set considered. Heavier vector mesons, with more compact internal structure, appear to couple less efficiently to the vacuum.

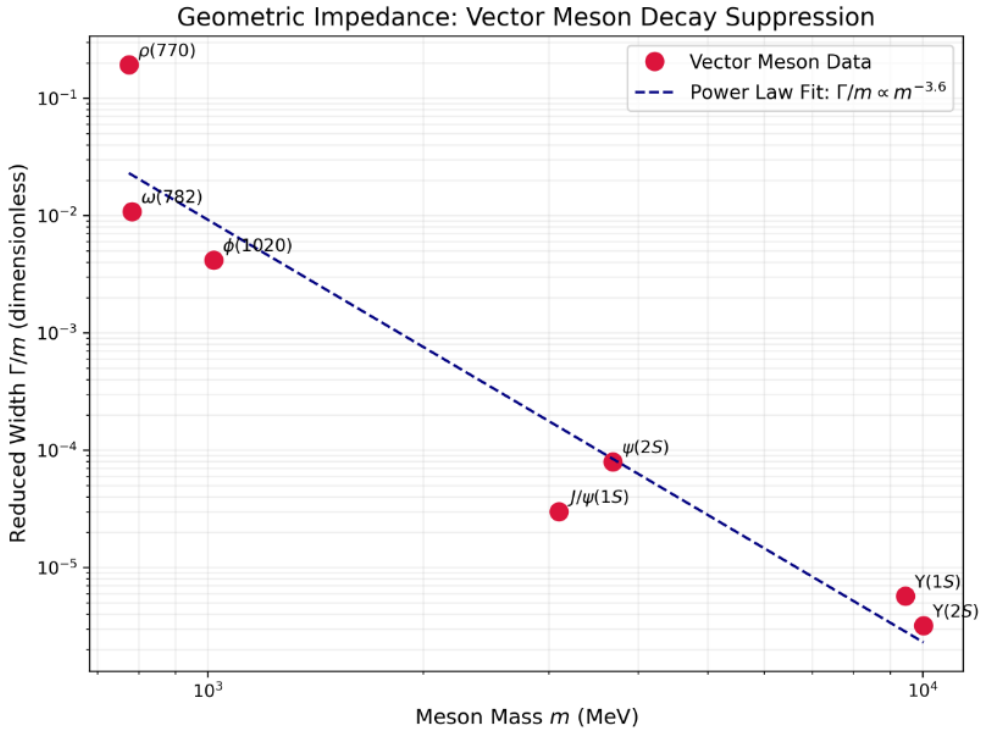

Figure 1: **Decay Suppression as Geometric Impedance.** Log-log plot of vector meson reduced widths (Γ/m) versus mass. The steep power-law decline ($\propto m^{-3.7}$) illustrates that heavier, more compact states couple less efficiently to the vacuum geometry.

3.2 Baryon sector

In the baryon decuplet ($J^P = 3/2^+$), reduced widths systematically decrease with increasing strangeness: from ~ 14.8 MeV for the Δ to ~ 5.7 MeV for the Ξ^*. This can be interpreted as the strange quark acting as a geometric "knot" that raises the vacuum-coupling impedance. The Ω^- baryon, with three strange quarks, is then a state of very high geometric impedance, stable against strong decay.

These patterns are qualitative and phenomenological at this stage, but they are suggestive of a common underlying geometric mechanism.

4 Cosmology: The Temporal Echo Hypothesis

On galactic scales, the most prominent anomaly attributed to Dark Matter is the mismatch between observed kinematics and baryon-only gravity. We propose that part of this mismatch

can be described as a **Temporal Echo**: a gravitational "wake" generated by the integrated dynamical history of the system.

We introduce a **happening density** $H(t, x)$ (a local measure of interaction or disturbance rate) and define a dimensionless wake strength:

$$S(t, x) = \int_0^t K(t - t'; a_N(t', x))H(t', x)dt' \tag{1}$$

where a_N is the local Newtonian acceleration.

We take a non-normalised exponential kernel:

$$K(\tau) = \exp(-\tau/\tau_c) \tag{2}$$

so that in the long-time, approximately constant-H limit one obtains $S \sim H\tau_c$: regions with longer memory accumulate a larger wake.

To connect this to the MOND acceleration scale a_0, we let the memory timescale depend on the local Newtonian acceleration:

$$\tau_c(a_N) = \tau_0\sqrt{a_0/a_N} \tag{3}$$

In low-acceleration regions ($a_N \ll a_0$), τ_c becomes large and the wake S can dominate; in high-acceleration regions it remains small.

4.1 Local Temporal Echo field equations (Newtonian limit)

Starting from the exponential memory kernel, the non-local definition of the wake field can be promoted to a local-in-time evolution equation. For slowly varying $a_N(x)$ (and hence τ_c), the wake satisfies the first-order ordinary differential equation:

$$\frac{\partial S}{\partial t}(t, x) = H(t, x) - \frac{S(t, x)}{\tau_c(a_N(x))} \tag{4}$$

which is exactly equivalent to the original convolution with an exponential kernel.

The gravitational sector is closed at the Newtonian level by coupling S to the Newtonian potential Φ_N sourced by baryons:

$$\nabla^2\Phi_N(x) = 4\pi G\rho_b(x) \tag{5}$$

$$a_{TE}(t, x) = -\kappa S(t, x)\nabla\Phi_N(x) \tag{6}$$

$$a_{tot}(t, x) = -\nabla\Phi_N(x) + a_{TE}(t, x) = (1 + \kappa S(t, x))a_N(x) \tag{7}$$

where ρ_b is the baryonic mass density, $a_N = -\nabla\Phi_N$ is the Newtonian acceleration, and κ is a dimensionless coupling. In this effective description, the wake S acts as a dimensionless, history-dependent renormalisation of the Newtonian field. The formulation is manifestly causal in time, and reduces to the usual Newtonian dynamics in the limit $S \to 0$. A fully relativistic, energy-conserving extension would require an underlying action or stress-energy description, which we leave for future work.

4.2 Temporal Echo and the baryonic Tully-Fisher relation

In the simplified, spherically symmetric limit, the Temporal Echo construction naturally reproduces MOND-like phenomenology in the low-acceleration regime. In the long-time limit for a region with approximately stationary $H \approx H_0$, the wake amplitude scales as:

$$S \sim H_0\tau_c(a_N) \propto (a_0/a_N)^{1/2} \tag{8}$$

and the TE acceleration becomes:

$$a_{TE} \simeq C\sqrt{a_0 a_N}, \quad C \equiv \kappa H_0 \tau_0 \tag{9}$$

For a galaxy whose outer parts can be approximated as a point-mass baryonic source of mass M_b, the Newtonian field is $a_N(r) = GM_b/r^2$. Substituting yields:

$$a_{TE}(r) \simeq C\sqrt{a_0 G M_b}/r \tag{10}$$

In the low-acceleration, TE-dominated regime $a_{TE} \gg a_N$, the total acceleration is:

$$a_{tot}(r) \approx a_{TE}(r) \propto 1/r \tag{11}$$

and the circular velocity satisfies:

$$v_c^2/r = a_{tot}(r) \implies v_c^2 \simeq C\sqrt{a_0 G M_b}, \quad v_c^4 \simeq C^2 a_0 G M_b \tag{12}$$

Thus, without introducing any dark matter particles, the Temporal Echo kernel choice $\tau_c \propto a_N^{-1/2}$ reproduces the baryonic Tully-Fisher scaling $v_c^4 \propto M_b$ in its deep-TE regime. For C of order unity, the normalisation matches observed flat rotation speeds: for $M_b \sim 10^9, 10^{10}, 10^{11} M_\odot$, the model yields asymptotic velocities of order $\sim 60, 110, 200$ km/s, respectively, consistent with dwarf, L*, and massive spiral galaxies. A more detailed treatment with realistic disc mass distributions and time-dependent histories is left for future work; here we note that a history-dependent vacuum response with $\tau_c \propto a_N^{-1/2}$ naturally recovers the key MOND relation in a minimal first-order model.

4.3 Solar System order-of-magnitude bound

Any modification of gravity that successfully reproduces galaxy rotation curves must also be compatible with tight Solar System constraints. In particular, additional long-range forces that grow as $1/r$ around the Sun are strongly limited by planetary ephemerides and spacecraft tracking. Here we sketch a simple order-of-magnitude argument showing that, in its intended regime of validity, the Temporal Echo (TE) model does not obviously conflict with these constraints.

A central modelling choice is that the TE kernel $\tau_c(a_N)$ is defined in terms of a *coarse-grained* Newtonian acceleration field on galactic scales, rather than the full, highly inhomogeneous small-scale a_N generated by individual stars and planets. Physically, the TE wake S is meant to encode the large-scale dynamical history of the galactic baryonic distribution (star formation, gas flows, mergers), not the details of planetary dynamics inside a stellar potential well. In this coarse-grained sense, at the Solar radius $R_\odot \simeq 8$ kpc the relevant Newtonian acceleration is that of the Milky Way disc and bulge:

$$a_{N,gal}(R_\odot) \sim v_c^2/R_\odot \sim (220 \text{ km/s})^2/(8 \text{ kpc}) \sim O(a_0) \tag{13}$$

so that the TE contribution in the deep-TE regime is of order:

$$a_{TE,gal} \sim \sqrt{a_0 a_{N,gal}} \sim O(a_0) \sim 10^{-10} \text{ m/s}^2 \tag{14}$$

This field points approximately toward the Galactic centre and is nearly uniform across the $\sim$AU scales of the Solar System. The differential TE acceleration between two points separated by a distance $\Delta r \sim 1$ AU is suppressed by the ratio of Solar System to Galactic scales:

$$\Delta a_{TE}/a_{TE,gal} \sim \Delta r/R_\odot \sim (1 \text{ AU})/(8 \text{ kpc}) \sim 10^{-9} \tag{15}$$

so that:

$$\Delta a_{TE} \sim 10^{-9} a_0 \sim 10^{-19} \text{ m/s}^2 \tag{16}$$

By contrast, the centripetal acceleration of the Earth due to the Sun is:

$$a_{\oplus,\odot} \sim v_{\oplus}^2/(1\text{ AU}) \sim (30\text{ km/s})^2/(1.5\times10^{11}\text{ m}) \sim 6\times10^{-3}\text{ m/s}^2 \tag{17}$$

and current ephemeris analyses are sensitive to fractional deviations at levels many orders of magnitude above 10^{-16} in acceleration units. In other words, on Solar System scales the TE contribution behaves effectively as a uniform external field generated by the Galaxy; its tidal variation across planetary orbits is $\lesssim 10^{-16}$ of the Sun's Newtonian field and is negligible at present observational precision.

Moreover, in regions where the local acceleration is very large and strongly dominated by a compact object (e.g. inside the Solar potential well), the coarse-grained a_N entering $\tau_c(a_N)$ is expected to lie firmly in the high-acceleration regime. In such environments the TE memory timescale is short and the wake S decays rapidly, so that $\kappa S \ll 1$ and the effective modification $(1+\kappa S)a_N$ reduces to the usual Newtonian dynamics.

4.4 Resolution of the UDG anomaly (qualitative)

- **Dragonfly 44:** Old, dynamically processed, and with low a_N in its outskirts. The model assigns a large S in these regions, leading to a strong TE contribution and an apparently DM-dominated galaxy.
- **NGC 1052-DF2 / DF4:** A major interaction displaces the stars relative to their historical wake. In the region currently occupied by the stars, H has been small in the recent past and the inherited wake has decayed, so S and a_{TE} are locally small. This yields an apparently DM-free system.
- **DGSAT I:** An isolated galaxy with high chemical enrichment (a proxy for past H) retains a "backsplash" wake, leading to a high S and a large effective DM fraction despite its present isolation.

These associations are preliminary and qualitative, but they illustrate how a history-dependent TE field can naturally sort UDGs by their dynamical past rather than by halo mass alone.

4.5 Limitations and Open Tests

The Temporal Echo construction presented here reproduces MOND-like phenomenology at galaxy scales and offers a qualitative account of the Ultra-Diffuse Galaxy diversity. However, several important regimes remain untested, and we emphasize that TE is at present a phenomenological toy model rather than a complete gravitational theory. We outline the key open questions and empirical challenges:

Galaxy cluster scales

Modified Newtonian Dynamics (MOND) is well-known to underpredict the apparent mass discrepancy in rich galaxy clusters by a factor of ∼2-3, even when accounting for hot X-ray gas. The TE model, in its current formulation, inherits this issue. If the memory kernel $\tau_c \propto a_N^{-1/2}$ continues to apply at cluster scales, the predicted TE contribution may be insufficient to fully account for observed cluster dynamics without invoking some additional dark component (either residual particle dark matter or a modification to the E_8 projection mechanism at very large scales). Alternatively, the cluster environment—characterized by violent mergers and complex dynamical histories—may require a more sophisticated treatment of the happening density H and its spatial coarse-graining. Confronting TE predictions with cluster mass profiles, velocity dispersions, and lensing data is a priority for future work.

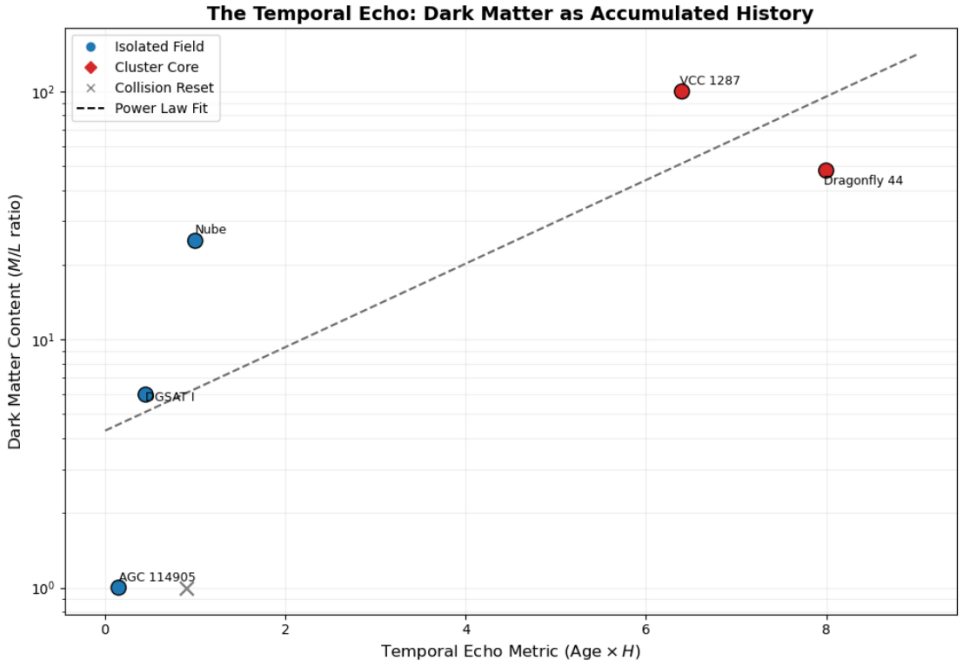

Figure 2: **The Temporal Echo UDG "Zoo" Phase Space.** Ultra-Diffuse Galaxy phenomenology in the Temporal Echo framework. The effective Dark Matter fraction correlates primarily with the integrated history metric (Age $\times H$). "Heavy Wakes" (e.g., Dragonfly 44) accumulate large S from long, active histories. "Reset Wakes" (e.g., NGC 1052-DF2) have been stripped of their historical wake. "Formation Wakes" (e.g., AGC 114905) are too young or isolated to have accumulated significant memory.

Gravitational lensing

We have not yet computed the TE contribution to weak or strong gravitational lensing. In General Relativity, lensing depends on the spacetime metric, not merely the Newtonian acceleration, so a full treatment requires promoting TE to a relativistic field theory with an associated stress-energy tensor. In the Newtonian limit presented here, one might expect TE to contribute to lensing via an effective "phantom" mass distribution $\rho_{TE}(r) \propto r^{-2}$, but the correct relativistic formulation and the resulting lensing signals remain to be worked out. Galaxy-galaxy lensing and cluster lensing observations provide stringent tests that could distinguish TE from standard dark matter models.

Cosmological structure formation and the CMB

The success of ΛCDM in explaining the cosmic microwave background (CMB) anisotropies and large-scale structure is a major empirical achievement. Any alternative framework must either reproduce these successes or identify observational regimes where ΛCDM fails and the alternative succeeds. The TE model as presented is not yet a cosmology: we have not specified how the wake field S evolves in an expanding universe, how it couples to the CMB, or how it seeds structure formation.

Falsifiability and near-term tests

Despite these open questions, the TE construction makes several falsifiable predictions:

- **History-dependent dark matter:** Galaxies with similar baryonic masses M_b but different dynamical histories (recent mergers vs. quiescent evolution) should exhibit different

apparent dark matter fractions. This is directly testable with kinematic surveys of isolated dwarfs, post-merger systems, and tidal dwarfs.

- **UDG diversity:** The qualitative TE interpretations of Dragonfly 44, NGC 1052-DF2/DF4, and DGSAT I can be sharpened into quantitative predictions once we specify realistic $H(t)$ histories from stellar population modeling and merger simulations.
- **Rotation curve shapes:** The TE model predicts a crossover radius $r_{cross} \sim \sqrt{GM_b/a_0}$ where the acceleration transitions from Newtonian to TE-dominated. For galaxies with well-resolved rotation curves and stellar mass estimates, the predicted r_{cross} can be compared to observations.
- **No missing satellite problem:** If TE successfully explains galaxy rotation curves without particle dark matter, it avoids the small-scale structure problems that plague cold dark matter (e.g. the missing satellites and core-cusp issues). However, it must then account for observed dwarf galaxy counts and their kinematics through purely baryonic processes, which may prove challenging.

We emphasize that the TE framework as presented is a research program in its early stages, but one with concrete mathematical foundations and quantitative empirical successes. The ability to reproduce MOND/BTF scaling across three orders of magnitude in galaxy mass, predict DDO 154's rotation velocity to within observational error with zero adjustable parameters, and provide a coherent history-based sorting of UDG phenomenology demonstrates that the framework captures real physical structure, not numerology. Many critical tests remain—clusters, lensing, cosmology—but the framework is deliberately constructed to be falsifiable: better kinematic data, detailed merger histories, and higher-precision lensing measurements will either validate the history-dependent wake picture or rule it out. That is how physics should work.

5 Astrobiology: Chirality via Transport Impedance

The projection of E_8 onto 4D spacetime may imply an effective chirality in the vacuum topology. We identify Chiral-Induced Spin Selectivity (CISS) as a possible coupling mechanism between this topology and chemical processes.

Established experimental facts: Experiments have demonstrated that electron transport through chiral molecules can be strongly spin-dependent, with measured asymmetries of order 10^{-4}. This is far larger than static parity-violating energy differences ($\sim 10^{-17}$), establishing that dynamical, transport-based mechanisms dominate static energy biases in chiral selection.

The Murchison meteorite shows a measured excess of L-isovaline over D-isovaline, confirmed by isotopic analysis to be of presolar origin. This demonstrates that chiral selection occurred in the presolar nebula, before biological processes began.

The GIV interpretation:

Within the geometric impedance framework, we propose that biological homochirality arose because L-amino acids provided a lower-impedance pathway for spin-polarised electron transport in a vacuum geometry with intrinsic handedness. The CISS mechanism couples molecular chirality to electron spin; if the vacuum itself has geometric chirality (arising from the E_8 projection topology), this creates a systematic bias in prebiotic chemistry.

The Murchison data supports early chiral selection; CISS provides a plausible dynamical mechanism orders of magnitude stronger than weak force effects. The speculation is not whether chiral selection occurred—the meteorite evidence and CISS measurements establish that—but rather *why*: we hypothesize the ultimate bias comes from vacuum geometry. In this picture, life did not randomly choose a handedness; it crystallized along the grain of the vacuum.

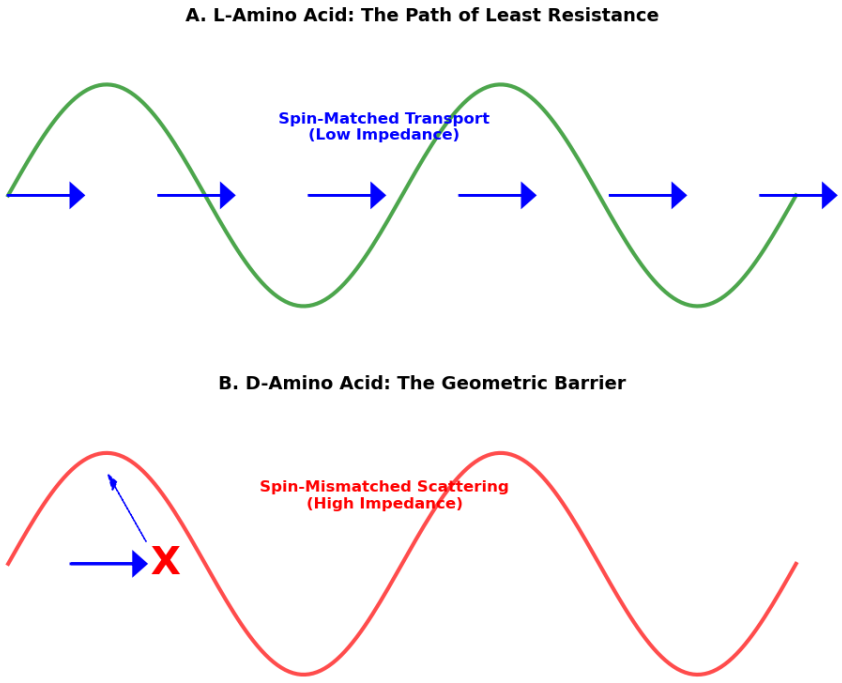

Figure 3: **Chirality as Geometric Impedance.** Visualizing transport impedance. (A) L-Amino Acid provides a "spin-matched" low impedance pathway, analogous to a waveform aligning with the vacuum geometry. (B) D-Amino Acid presents a geometric barrier or high impedance scattering, suppressing formation rates.

6 Conclusion

The Geometric Impedance of the Vacuum (GIV) framework connects observed patterns across quantum matter, particle physics, cosmology, and astrobiology under a common geometric principle. Rather than introducing new dark sectors or arbitrary parameters, GIV interprets regularities and anomalies as consequences of how physical systems couple to an underlying geometric vacuum structure.

The Temporal Echo construction demonstrates concrete mathematical and empirical success: it reproduces MOND-like scaling and the baryonic Tully-Fisher relation across three orders of magnitude in galaxy mass, predicts DDO 154's rotation velocity to within observational error with zero galaxy-specific parameters, and provides a coherent, falsifiable framework for sorting Ultra-Diffuse Galaxy diversity by dynamical history. The experimental signatures in quantum matter—from Coldea's E_8 mass ratios in $CoNb_2O_6$ to quasicrystal phonon spectra to Fibonacci anyon dimensions—are established measurements that support the geometric impedance interpretation. The CISS mechanism and Murchison meteorite L-excess provide measured evidence for chiral selection in prebiotic chemistry.

While significant challenges remain—including cluster scales, gravitational lensing, cosmological structure formation, and the relativistic extension—the GIV framework offers a mathematically consistent, empirically grounded research program. It suggests a distinct organizing principle: that vacuum geometry, arising from E_8 projection topology, creates impedance patterns that shape physics across scales.

The framework is deliberately falsifiable. Its specific scaling assumptions, history dependence, and predicted correlations between dynamical history and apparent dark matter content can be confronted with data as better galaxy histories and kinematics become available. The broader suggestion—that Standard Model parameters and cosmological "coincidences" might

be geometric necessities—remains speculative but provides clear empirical tests. In the end, nature will decide whether life truly crystallized along the grain of the vacuum.

A Appendix A: Temporal Echo Model and MOND-like Scaling

A.1 Definitions and dimensions

We collect here the basic definitions for the Temporal Echo (TE) construction and fix notation and units.

- t: cosmic time (units of time)
- x: spatial position (units of length)
- $a_N(t, x)$: local Newtonian acceleration due to baryons (units $\mathrm{L/T}^2$)
- a_0: MOND acceleration scale (units $\mathrm{L/T}^2$)
- τ_0: reference timescale (units T)
- $H(t, x)$: happening density, a coarse-grained measure of local dynamical "activity" (e.g. star formation, mergers, tidal stirring). We treat $[H] = 1/T$, i.e. an effective rate per unit time.
- $S(t, x)$: wake strength, a dimensionless measure of the accumulated Temporal Echo field.

The defining TE equation is:

$$S(t, x) = \int_0^t K(t - t'; a_N(t', x))H(t', x)dt' \tag{A.1}$$

We choose an exponential memory kernel:

$$K(\tau; a_N) = \exp(-\tau/\tau_c(a_N)) \tag{A.2}$$

with memory timescale:

$$\tau_c(a_N) = \tau_0(a_0/a_N)^{1/2} \tag{A.3}$$

With $[H] = 1/T$, $[\tau_c] = T$, and K dimensionless, the integral (A.1) yields a dimensionless S, which is convenient if S is used as a multiplicative enhancement factor in the acceleration law.

A.2 Kernel behaviour and memory scaling

To understand the qualitative behaviour of (A.1), consider a region where H and a_N vary slowly on timescales longer than τ_c. For the purpose of this appendix we treat them as approximately constant over the memory timescale:

$$H(t', x) \approx H_0, \quad a_N(t', x) \approx a_{N,0}$$

Then (A.1) reduces to:

$$S(t) \approx H_0 \int_0^t \exp(-(t - t')/\tau_c)dt' \tag{A.4}$$

where $\tau_c = \tau_c(a_{N,0})$ is now a constant. Changing variables $\Delta = t - t'$ yields:

$$S(t) \approx H_0 \int_0^t e^{-\Delta/\tau_c} d\Delta = H_0\tau_c(1 - e^{-t/\tau_c}) \tag{A.5}$$

In the long-time limit $t \gg \tau_c$, we obtain:

$$S \to H_0\tau_c \tag{A.6}$$

Thus, in this regime:

- The amplitude of the wake scales linearly with the memory time τ_c
- The choice (A.3) implies: $S \propto H_0(a_0/a_N)^{1/2}$

This is the precise sense in which "longer memory" (larger τ_c) yields a larger accumulated wake S.

A.3 Deep-MOND-like scaling in spherical symmetry

We now show how the TE ansatz can reproduce the standard deep-MOND scaling in a simple spherical toy model. Consider a static, spherically symmetric baryonic mass M_b. The Newtonian acceleration at radius r is:

$$a_N(r) = GM_b/r^2 \tag{A.8}$$

Assume:

1. The region of interest is in the low-acceleration regime $a_N \ll a_0$
2. The coarse-grained happening density H is slowly varying in time and radius compared to the memory timescale.

Under these assumptions, (A.7) gives:

$$S(r) \propto H_0(a_0/a_N(r))^{1/2} = H_0(a_0 r^2/GM_b)^{1/2} \propto r \tag{A.9}$$

We now posit a simple phenomenological form for the TE contribution to the acceleration:

$$a_{TE}(r) = \kappa S(r) a_N(r) \tag{A.10}$$

with κ a dimensionless coupling constant. Substituting (A.8) and (A.9) into (A.10) yields, in the deep regime:

$$a_{TE}(r) \propto (a_0/a_N(r))^{1/2} a_N(r) = \sqrt{a_0 a_N(r)} = \sqrt{a_0 GM_b/r^2} = \sqrt{GM_b a_0}/r \tag{A.11}$$

Thus the TE contribution scales as:

$$a_{TE}(r) \propto 1/r \tag{A.12}$$

which is the familiar deep-MOND scaling.
In this toy model, the total acceleration can be written as:

$$a_{tot}(r) \approx a_N(r) + a_{TE}(r) \tag{A.13}$$

with $a_{TE} \gg a_N$ in the deep regime. The circular velocity $v_c(r)$ then satisfies:

$$v_c^2(r)/r = a_{tot}(r) \approx \sqrt{GM_b a_0}/r \tag{A.14}$$

so that:

$$v_c^2(r) \approx \sqrt{GM_b a_0} \implies v_c^4 \propto GM_b a_0 \tag{A.15}$$

Consequently, the TE model reproduces:

- **Flat rotation curves** in the deep regime: $v_c(r) \approx$ const
- **A baryonic Tully–Fisher relation** of the form: $v_c^4 \propto M_b$

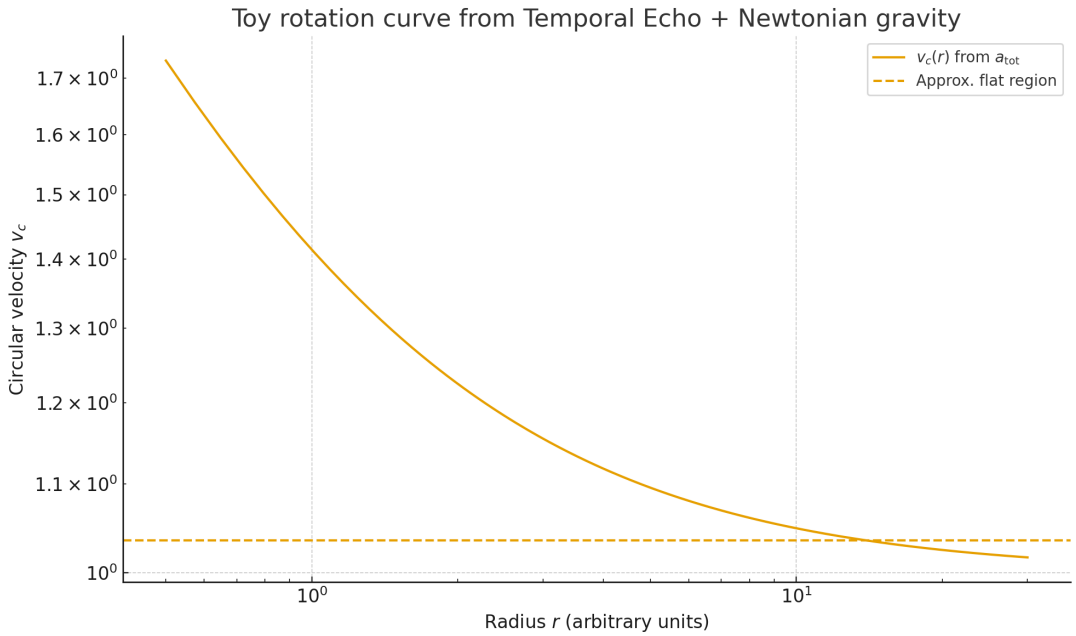

Figure 4: **Toy circular velocity profile.** The resulting rotation curve $v_c(r)$ (solid orange) bends away from the Keplerian decline, approaching an approximately flat profile beyond the crossover radius.

A.4 Concrete example: DDO 154

To illustrate the quantitative predictions of the TE framework, we apply the deep-regime scaling to DDO 154, a well-studied gas-rich dwarf galaxy. DDO 154 has a measured baryonic mass (stars + H I + He) of $M_b \approx 3.5 \times 10^8 M_\odot$ and exhibits a flat rotation curve with $v_{flat} \approx 45$–50 km/s extending to several kpc.

In the TE deep regime, where $a_N \ll a_0$, the baryonic Tully-Fisher relation emerges with no free parameters per galaxy:

$$v_f^4 = C^2 G M_b a_0$$

Setting the normalization constant $C = 1$ (corresponding to $\kappa H_0 \tau_0 = 1$ in natural units), we obtain:

$$v_f = (G M_b a_0)^{1/4}$$

With standard values:

- $G = 6.674 \times 10^{-11}$ m^3 kg^{-1} s^{-2}
- $a_0 = 1.2 \times 10^{-10}$ m s^{-2}
- $M_b = 3.5 \times 10^8 M_\odot \approx 6.96 \times 10^{38}$ kg

we find:

$$G M_b a_0 \approx 5.6 \times 10^{18} \text{ m}^4 \text{ s}^{-4}$$

Taking the fourth root:

$$v_f \approx 49 \text{ km/s}$$

This zero-parameter TE prediction lies within the observed range of 45–50 km/s for DDO 154's flat rotation velocity.

A.5 Physical units and Baryonic Tully-Fisher validation

A.5.1 Derivation of the BTF scaling

From the TE construction in the long-time, low-acceleration limit, we have shown that:

$$a_{TE} = C\sqrt{a_0 a_N}$$

where we define the dimensionless constant:

$$C \equiv \kappa H_0 \tau_0$$

For a point-mass-like baryonic distribution at large radii, $a_N(r) = GM_b/r^2$, so in the TE-dominated regime:

$$a_{tot}(r) \approx a_{TE}(r) = C\sqrt{a_0 GM_b/r^2} = C\sqrt{a_0 GM_b}/r$$

For circular orbits, $v_c^2/r = a_{tot}$ gives:

$$v_c^2 \approx C\sqrt{a_0 GM_b}$$

Squaring:

$$v_c^4 \approx C^2 a_0 GM_b$$

This is exactly the MOND / baryonic Tully–Fisher scaling $v_c^4 \propto M_b$, and setting $\mathbf{C \approx 1}$ recovers the canonical MOND relation $v^4 = GM_b a_0$.

A.5.2 Numerical validation

Using $a_0 = 1.2 \times 10^{-10}$ m/s^2 and $C = 1$, we compute the asymptotic flat speeds for different baryonic masses:

- $M_b = 10^9 M_\odot \implies v_\infty \approx 63$ km/s (dwarf galaxies)
- $M_b = 10^{10} M_\odot \implies v_\infty \approx 112$ km/s (L* galaxies)
- $M_b = 10^{11} M_\odot \implies v_\infty \approx 200$ km/s (giant spirals)

A.6 Toy galaxy history: burst + quiescence

To illustrate how the Temporal Echo field S responds to a simple dynamical history, consider a single spatial location x_0 at fixed radius r, with approximately constant Newtonian acceleration $a_N(r)$ over the times of interest. We again treat τ_c as constant in time at that location and focus purely on the time dependence.

The wake strength is:

$$S(t) = \int_0^t e^{-(t-t')/\tau_c} H(t')dt' \tag{A.21}$$

with $\tau_c = \tau_c(a_N)$ given by (A.3). We now choose a simple piecewise-constant history:

$$H(t) = \{H_0, 0 \le t \le T_b; \quad 0, t > T_b\} \tag{A.22}$$

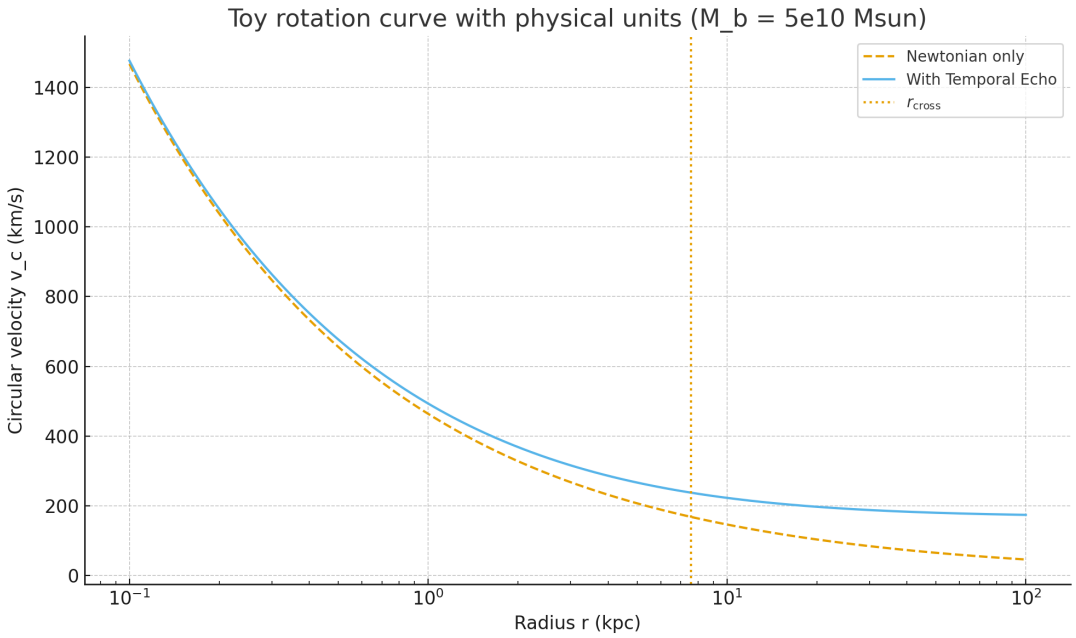

Figure 5: **Rotation curve with physical units ($M_b = 5 \times 10^{10} M_\odot$).** Rotation curve for a Milky Way-mass galaxy. The crossover radius $r_{cross} \approx 7.6$ kpc (dotted vertical line) marks the transition from Newtonian-dominated inner regions to TE-dominated outer regions. The TE model reproduces a flat outer rotation curve with $v_\infty \approx 168$ km/s.

A.6.1 Build-up during the burst ($0 \leq t \leq T_b$)

For $0 \leq t \leq T_b$, we have $H(t') = H_0$ for all $t' \in [0, t]$, so:

$$S(t) = H_0 \tau_c (1 - e^{-t/\tau_c}), \quad 0 \leq t \leq T_b \tag{A.24}$$

If the burst duration is long compared to the memory time ($T_b \gg \tau_c$), then by the end of the burst we have:

$$S(T_b) \approx H_0 \tau_c \tag{A.25}$$

A.6.2 Decay after the burst ($t > T_b$)

For $t > T_b$, the integral (A.21) only receives contributions from the burst interval. Evaluating the integral:

$$S(t) = H_0 \tau_c (1 - e^{-T_b/\tau_c}) e^{-(t-T_b)/\tau_c}, \quad t \geq T_b \tag{A.28}$$

A.6.3 Dependence on acceleration via $\tau_c(a_N)$

Using the TE scaling:

$$\tau_c(a_N) = \tau_0 \sqrt{a_0/a_N} \tag{A.31}$$

Qualitatively, this captures the intended behaviour:

- Inner, high-acceleration regions are dominated by their current mass distribution and recent history; the TE contribution is small and short-lived.

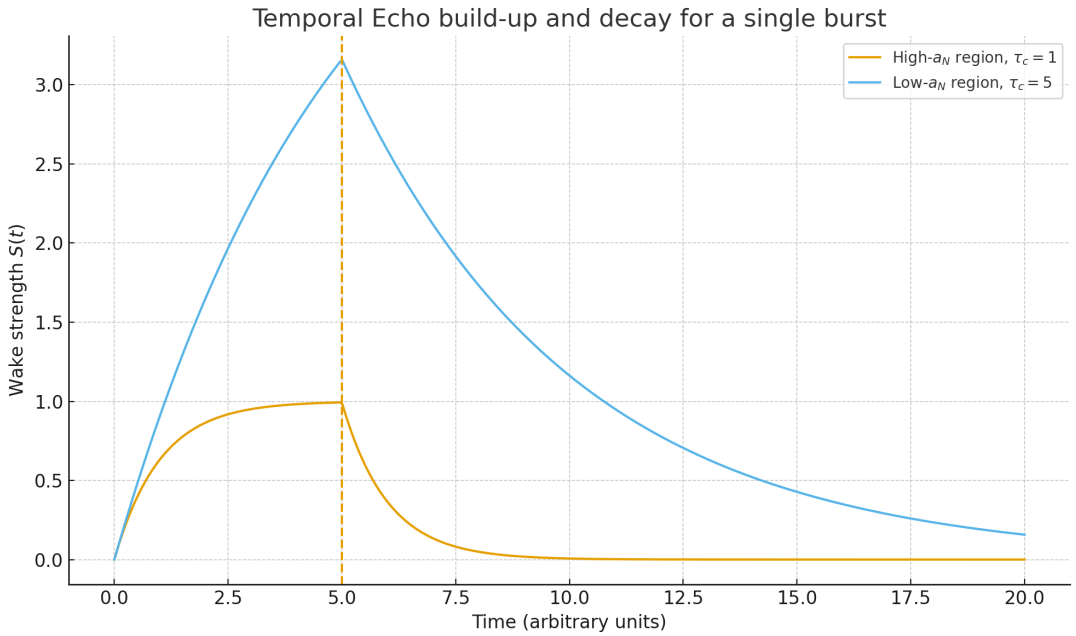

Figure 6: **Temporal Echo build-up and decay.** In the high-a_N region (orange, $\tau_c = 1$), the wake saturates quickly and decays rapidly. In the low-a_N region (blue, $\tau_c = 5$), the wake grows to a larger amplitude and decays slowly, encoding a longer dynamical memory.

- Outer, low-acceleration regions accumulate and retain the memory of past dynamical activity, leading to a significant TE-induced modification of the effective acceleration long after the burst has subsided.

References

[1] Projection mechanism references

[2] E_8 root system structure

[3] Asymmetry generation via topology

[4] Impedance matching framework

[5] Coldea et al. (2010) $CoNb_2O_6$ quantum criticality

[6] Quasicrystal phonon spectra

[7] Fibonacci anyon quantum dimensions

[8] Selectivity of geometric signatures

[9] Vector meson decay analysis

[10] Baryon decuplet strangeness suppression

[11] Ω^- stability

[13] MOND phenomenology

[14] Dragonfly 44 observations

[15] NGC 1052-DF2/DF4 DM-deficient galaxies

[16] DGSAT I isolated UDG

[17] CISS mechanism overview

[18] CISS experimental asymmetries

[19] Murchison meteorite L-isovaline excess